

Numerical Heat Transfer, Part A: Applications

An International Journal of Computation and Methodology

ISSN: (Print) (Online) Journal homepage: <https://www.tandfonline.com/loi/unht20>

Numerical investigation of steady state laminar natural convection of power-law fluids in side-cooled trapezoidal enclosures heated from the bottom

S. P. Malkeson, S. Alshaaili & N. Chakraborty

To cite this article: S. P. Malkeson, S. Alshaaili & N. Chakraborty (2023) Numerical investigation of steady state laminar natural convection of power-law fluids in side-cooled trapezoidal enclosures heated from the bottom, Numerical Heat Transfer, Part A: Applications, 83:7, 770-789, DOI: [10.1080/10407782.2022.2157353](https://doi.org/10.1080/10407782.2022.2157353)

To link to this article: <https://doi.org/10.1080/10407782.2022.2157353>



© 2023 The Author(s). Published with license by Taylor & Francis Group, LLC.



Published online: 17 Jan 2023.



Submit your article to this journal [↗](#)



Article views: 653



View related articles [↗](#)



View Crossmark data [↗](#)



Citing articles: 1 View citing articles [↗](#)



Numerical investigation of steady state laminar natural convection of power-law fluids in side-cooled trapezoidal enclosures heated from the bottom

S. P. Malkeson^a, S. Alshaaili^b, and N. Chakraborty^b 

^aSchool of Engineering, Liverpool John Moores University, United Kingdom; ^bSchool of Engineering, Newcastle University, Newcastle upon Tyne, United Kingdom

ABSTRACT

Laminar, steady-state, natural convection of power-law fluids in 2-D trapezoidal enclosures with a heated bottom wall, adiabatic top wall and cooled inclined sidewalls has been analyzed for the first time based on numerical simulations for a range of different values of nominal Rayleigh number (i.e. $10^3 \leq Ra \leq 10^5$), power-law index (i.e. $0.6 \leq n \leq 1.8$), nominal Prandtl number (i.e. $Pr = 10, 10^2, 10^3$) and sidewall inclination angle (i.e. $30^\circ \leq \phi \leq 60^\circ$). It has been found that the mean Nusselt number \overline{Nu} increases with increasing nominal Rayleigh number Ra (up to a 187% increase for $n = 0.6$ and up to 2.3% increase for $n = 1.8$ between $Ra = 10^3$ and 10^5) and decreasing power-law index n (up to a 4.1% increase for $Ra = 10^3$ and up to 193% increase for $Ra = 10^5$ between $n = 0.6$ and 1.8) due to the strengthening of advective transport. Moreover, an increase in the sidewall inclination angle ϕ leads to a decrease in \overline{Nu} (approximately 44% decrease for $Ra = 10^3$ across values of n and up to 33% decrease for $Ra = 10^5$ across values of n) due to an increase in the area for heat loss from the cavity. It has been found that \overline{Nu} does not vary significantly with the values of Pr considered in the current study. Furthermore, a new correlation for the mean Nusselt number \overline{Nu} in this configuration has been identified which provides adequate approximation of the corresponding values obtained from the simulations.

ARTICLE HISTORY



Received 12 October 2022
Revised 7 December 2022
Accepted 7 December 2022

KEYWORDS

Natural convection; Nusselt number; power-law fluid; trapezoidal enclosures

1. Introduction

Natural convection of shear-thinning and shear-thickening fluids in enclosed spaces has a broad range of applications in cooling of electronics, food and chemical processing, solar and nuclear power systems. Shear-thinning (shear-thickening) fluids are a special type of inelastic non-Newtonian fluid, which show a decrease (increase) in viscosity with an increasing shear rate. The majority of synthetic and biological fluids exhibit shear-thinning (e.g., ketchup, blood, silicone oils, and coatings) and shear-thickening (e.g., mixtures of corn starch and water, so-called “bullet-proof” custard) behaviors. Recently, Darbouli et al. [1] reported that 0.1–0.2% aqueous solutions of xanthan gum exhibit shear-thinning behavior and a significant enhancement in the strength of convection in comparison to Newtonian fluids (e.g., water) has been observed for laminar Rayleigh-Bénard convection in cylindrical enclosures. The addition of a small amount of high molecular weight polymer in water-based solvents often exhibits shear-thinning behavior

CONTACT S. P. Malkeson  s.p.malkeson@ljmu.ac.uk  School of Engineering, Liverpool John Moores University, Liverpool, L3 3AF, United Kingdom

© 2023 The Author(s). Published with license by Taylor & Francis Group, LLC.

This is an Open Access article distributed under the terms of the Creative Commons Attribution-NonCommercial-NoDerivatives License (<http://creativecommons.org/licenses/by-nc-nd/4.0/>), which permits non-commercial re-use, distribution, and reproduction in any medium, provided the original work is properly cited, and is not altered, transformed, or built upon in any way.

Nomenclature

C	specific heat capacity, $\text{J kg}^{-1}\text{K}^{-1}$	T_H	temperature of the heated bottom wall, K
C_1, C_2	model parameter	u_i	i^{th} component of velocity m s^{-1}
e_{ij}	strain rate tensor, s^{-1}	U_2	dimensionless vertical velocity ($u_2.L/\alpha$)
f_l	ratio of thicknesses of hydrodynamic to thermal boundary layers [-]	x_i	i^{th} component of spatial coordinate m
g	acceleration due to gravity, m s^{-2}	Greek	
Gr	Grashof number	α	thermal diffusivity, $\text{m}^2 \text{s}^{-1}$
h	heat transfer coefficient, $\text{W m}^{-2} \text{K}^{-1}$	β	thermal expansion coefficient, K^{-1}
H	height of the trapezoidal enclosure, m	δ	hydrodynamic boundary layer thickness, m
k	thermal conductivity, $\text{W m}^{-1} \text{K}^{-1}$	δ_{th}	thermal boundary layer thickness, m
K	consistency index, $\text{kg m}^{-1} \text{s}^{-1}$	δ_{ij}	Kronecker delta
L	length of heated bottom wall of trapezoidal enclosure, m	ρ	density, kg m^{-3}
min	minimum value	μ	dynamic viscosity, $\text{kg m}^{-1} \text{s}^{-1}$
max	maximum value	μ_a	apparent viscosity, $\text{kg m}^{-1} \text{s}^{-1}$
n	power-law index	μ_{eff}	effective viscosity, $\text{kg m}^{-1} \text{s}^{-1}$
Nu	local Nusselt number	ϑ	characteristic vertical velocity component, m s^{-1}
\bar{Nu}	mean Nusselt number	ϕ	inclination angle of trapezoidal enclosure sidewall, $^\circ$
p	pressure, $\text{kg m}^{-1} \text{s}^{-2}$	ψ	stream function, $\text{m}^2 \text{s}^{-1}$
Pr	Prandtl number	Ψ	nondimensional stream function
q_w	heat flux at the bottom wall, W m^{-2}	θ	nondimensional temperature
R^2	coefficient of determination	τ_{ij}	stress tensor, $\text{kg m}^{-1} \text{s}^{-2}$
Ra	Rayleigh number	ΔT	temperature difference between the hot and cold walls, K
Ra_{eff}	effective Rayleigh number		
T	temperature, K		
T_c	temperature of the cooled inclined side-walls, K		

which can be approximated as a power-law over a range of shear rates. Thus, for a first approximation, a reasonable way to include non-Newtonian shear viscosity variations is through a simple power-law type Generalized Newtonian Fluid (GNF) model [2]. The onset of convection of power-law fluids in rectangular enclosures with differentially heated horizontal walls with heated bottom and adiabatic side walls (i.e., known as Rayleigh-Bénard convection) was analyzed by Lamsaadi et al. [3, 4] and Aloui et al. [5]. The heat transfer characteristics beyond the critical condition for the onset of convection in the same configuration have also been analyzed by Ohta et al. [6] and Inaba et al. [7] for power-law fluids and they reported augmentation of convective transport with a decrease in power-law exponent. Several studies by Chakraborty and coworkers [8–15] analyzed the effects of power-law exponent, aspect ratio, nominal Rayleigh number and nominal Prandtl number on the mean Nusselt number for Rayleigh-Bénard convection in rectangular and cylindrical annular spaces for both constant wall heat flux (CWHF) and constant wall temperature (CWT) boundary conditions for differentially heated horizontal walls. The simulation data and scaling analysis were used by Chakraborty and coworkers [8–15] to propose the correlations for the mean Nusselt number. Natural convection of power-law fluids in the differentially heated vertical side walls was extensively numerically analyzed by several researchers [16–23] and the effects of nominal Prandtl number, Rayleigh number and aspect ratio on the mean Nusselt number in rectangular and cylindrical annular enclosures with differentially heated vertical walls have been addressed and correlations for the mean Nusselt number have been proposed. Several studies (e.g. [24–30] and references therein) also focused on the analyses of natural convection of Newtonian fluids in rectangular enclosures (for different aspect ratios). Despite extensive studies of natural convection in rectangular enclosures, relatively limited attention has been directed to the natural convection in non-rectangular enclosures. The Rayleigh-Bénard convection (i.e., heated bottom wall and cooled top wall with adiabatic inclined side walls) within

trapezoidal enclosures filled with viscoplastic fluid has been analyzed by Aghighi et al. [31] across a range of parameters (i.e., side wall inclination angle, Rayleigh number and Prandtl number). Furthermore, Hussein et al. [32] considered the 3-D unsteady natural convection in an inclined trapezoidal air-filled cavity where the variations of local and average Nusselt numbers are presented. They [32] further observed that the flow circulation strengthens and the mean Nusselt number increases with increasing Rayleigh number. Iyican et al. [33] used both experimental and numerical means to analyze natural convection of Newtonian fluids in inclined cylindrical trapezoidal enclosures made up of cylindrical cold top and hot bottom walls and plane side walls. Lam et al. [34] analyzed natural convection in trapezoidal cavities with vertical sidewalls and inclined cold top and horizontal hot bottom walls. By contrast, Karyakin [35] analyzed natural convection of Newtonian fluids in trapezoidal enclosures with parallel horizontal walls and inclined side walls. Lee [36, 37] and Peric [38] numerically analyzed natural convection in trapezoidal enclosures with insulated horizontal top and bottom walls for Rayleigh numbers up to 10^5 and their analyses were subsequently extended by Sadat and Salagnac [39] and Kuyper and Hoogendoorn [40] for higher values of Rayleigh number. Moukalled and Acharya [41–43] and Moukalled and Darwish [44] numerically analyzed natural convection in trapezoidal enclosures with several different configurations involving partitions and baffles. The effects of Rayleigh number, Prandtl number and inclination angle of the top wall on natural convection of Newtonian fluids within trapezoidal enclosures with partitions and baffles have been analyzed by da Silva et al. [45] and the simulation data was used to propose a correlation for the mean Nusselt number. Basak et al. [46] numerically analyzed natural convection of Newtonian fluids within trapezoidal enclosures with bottom wall subjected to uniform heat flux and linearly heated sidewalls in the presence of an insulated top wall. Unsteady natural convection of Newtonian fluids in an isosceles trapezoidal enclosure with differentially heated horizontal walls heated from below was analyzed numerically by Tracy and Crunkleton [47]. Natural convection of Newtonian fluids within a trapezoidal enclosure with a flexible partition has recently been analyzed for different Rayleigh numbers by Mehryan et al. [48] who also analyzed the flow-induced stresses on the flexible partition.

Several studies focused on the heat transfer behavior of Newtonian fluids in trapezoidal/non-rectangular enclosures where natural convection and mixed convection (i.e., where both natural and forced convection) have been analyzed for nanofluids and magnetohydrodynamic (MHD) flows. Haq et al. [49] presented a computational analysis of natural convection of water-based carbon nanotubes in a trapezoidal enclosure partially heated from the horizontal bottom wall and cooled by inclined sidewalls. They reported an augmentation of heat transfer due to natural convection of nanofluids involving carbon nanotubes [49]. This analysis was subsequently extended to account for water based CuO nanofluids within trapezoidal enclosure where a heated obstacle is placed at the center of the enclosure [50]. They reported a decrease in heat transfer rate with increasing volume fraction of CuO nanoparticles. Saleh et al. [51] analyzed natural convection of water–Cu and water– Al_2O_3 nanofluids in trapezoidal enclosures with differentially heated inclined sidewalls and reported heat transfer enhancements due to the presence of nanoparticles. Esfe et al. [52] analyzed Rayleigh–Bénard convection of carbon nanotubes within trapezoidal enclosures and revealed that the mean Nusselt number decreases with increasing inclination angle for sidewalls for small Rayleigh number values ($\leq 10^4$) but a non-monotonic trend of mean Nusselt number with inclination angle is obtained for large Rayleigh numbers ($\sim 10^6$) for all solid volume fractions. Ghoben and Hussein [53] considered unsteady natural convection of (Al_2O_3 –water) nanofluids inside a 3-D triangular cross-sectional enclosure, which was heated differentially with the vertical walls kept at different constant temperatures, with and without internal cylinders in different arrangements (i.e., no cylinder, single cylinder, double cylinder aligned, and double cylinder not aligned). Ghoben and Hussein [53] found that a higher nanoparticle volume fraction leads to an increase in Nusselt number, which also increases with increasing Rayleigh number. Moreover, for the cases with internal cylinders, the average Nusselt number was greater for the case of double cylinders than in the single cylinder arrangement. Hussein [54] investigated entropy generation of the

mixed convection in a 3-D right-angle triangular air-filled enclosure where the flow field is significantly influenced by the direction of the moving wall and that the Bejan number decreases with increasing Richardson number. Laouira et al. [55] numerically investigated heat transfer characteristics inside a horizontal channel with an open trapezoidal enclosure, which is subjected to different lengths of heat sources. They found that the distribution of isotherms is significantly dependent on the heat source length and both local and mean Nusselt numbers increase as the length of the heat source increases [55]. Kareem et al. [56] numerically analyzed mixed convection in a 2-D trapezoidal lid-driven nanofluid filled enclosure heated from below and nanofluids have been found to yield higher Nusselt number compared to pure water.

Hossain and Abdul Alim [57] numerically analyzed MHD mixed convection of Newtonian fluids in trapezoidal enclosures heated from below and cooled by side walls and reported that Rayleigh number, Prandtl number, Hartman number and inclination angle have significant effects on the mean Nusselt number in this configuration. Gibanov et al. [58] computationally analyzed natural convection of micropolar fluids in trapezoidal enclosures with heated bottom and cooled inclined sidewalls and reported that the vortex viscosity parameter leads to attenuation of heat transfer rate. Ahmed et al. [59] numerically investigated MHD mixed convection in trapezoidal enclosures filled with water-based micropolar nanofluids in a configuration heated from below and cooled by side walls and it was reported that the mean Nusselt number increases when Richardson number decreases, and the nanoparticle solid volume fraction increases, but it decreases as the length of the heat source at the bottom wall increases. Ali et al. [60] numerically analyzed mixed MHD convection due to a rotating circular solid cylinder in a trapezoidal nanofluid filled enclosure which was saturated with a porous media. They found that the mean Nusselt number rises with increasing Darcy number, Hartmann number, thermal conductivity ratio and cylinder radius, but decreases with increasing Richardson number [60]. Hussein et al. [61] considered laminar 2-D mixed convection in porous medium within a trapezoidal enclosure with a rotating inner circular cylinder and a sinusoidal bottom wall for their numerical study. They also found that Nusselt number increases with increasing Rayleigh and Darcy numbers, solid volume fraction, inner cylinder radius and the angular rotational velocity of the cylinder, while it decreases as the porous layer thickness and the number of undulations increase.

Despite the studies of heat transfer characteristics in different shaped cavities, with different boundary conditions, for both natural and mixed convection in Newtonian and non-Newtonian fluids, to the best of the authors' knowledge, the natural convection in power-law fluids in a trapezoidal enclosure with heated bottom wall, cooled inclined sidewalls and an adiabatic top wall is yet to be analyzed in detail and a correlation for the mean Nusselt number in the aforementioned configuration is yet to be proposed. However, this information is fundamentally important for engineering applications ranging from electronic cooling to food and chemical processing to name a few. This analysis fills the aforementioned gap in the existing literature. Therefore, the objectives of the current study are as follows:

1. To investigate the influence of the geometry of the enclosure, nominal Rayleigh number Ra , nominal Prandtl number Pr and power law index n on the steady laminar natural convection behavior in power-law fluids in a trapezoidal enclosure with heat bottom wall, cooled inclined sidewalls, and an adiabatic top wall.
2. To identify a correlation for the mean Nusselt number \overline{Nu} in the considered configuration across the range of Ra , Pr , n , and ϕ examined for steady state laminar convection.

The remainder of the article is organized as follows. In the next section, the mathematical background and numerical implementation pertaining to this analysis are presented. This is followed by the presentation of results and their discussion. In the final section of this article, the main findings are summarized, and conclusions are drawn.

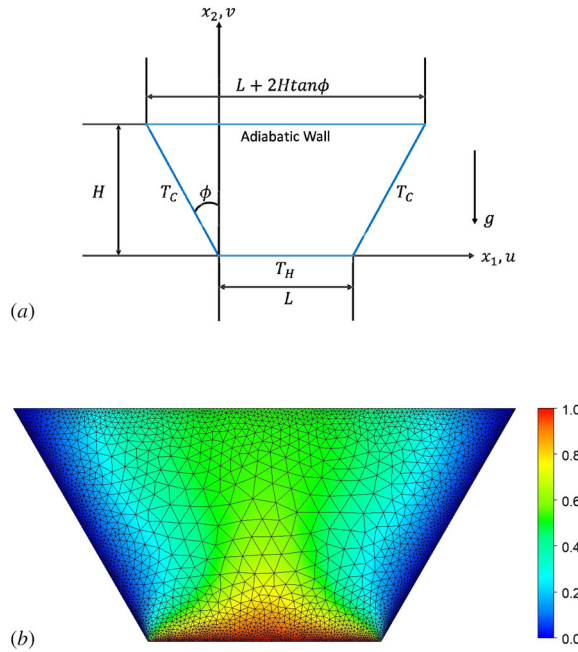


Figure 1. (a) Considered configuration, and (b) the nondimensional temperature $\theta = (T - T_C) / (T_H - T_C)$ field for the $Ra = 10^6$, $Pr = 10^2$, $n = 1.8$, $\theta = 30^\circ$ case with the mesh superimposed.

2. Mathematical background

The schematic of the configuration considered in the current analysis is provided in Figure 1a where H is the height of the trapezium, L is the length of the bottom heated wall, and ϕ is the inclination angle of the sidewall. The heated bottom wall is kept at a temperature T_H . The two inclined sidewalls are kept at a temperature T_C . It is assumed that $T_H > T_C$ for the current analysis. The top wall is taken to be adiabatic. All walls are considered to be no-slip and impenetrable. The flow is assumed to be laminar, incompressible, steady, and 2-D (i.e., the physical flow domain is assumed to be an infinitely long channel and the third dimension is considered not to affect the flow field). The conservation equations for mass, momentum, and energy take the following form for the current study [8–23]:

$$\partial u_i / \partial x_i = 0 \quad (1a)$$

$$\rho u_j (\partial u_i / \partial x_j) = -(\partial p / \partial x_i) + \delta_{2i} \rho g \beta (T_H - T_C) + \partial \tau_{ij} / \partial x_j \quad (1b)$$

$$\rho u_j C (\partial T / \partial x_j) = k (\partial^2 T / \partial x_j \partial x_j) \quad (1c)$$

where u_i (x_i) is the i^{th} component of velocity (spatial coordinate), ρ is density, p is pressure, g is acceleration due to gravity, β is the volume expansion coefficient, τ_{ij} is the stress tensor, C is specific heat, T is the temperature, and k is thermal conductivity. In Eqs. (1b) and (1c) the terms on the left-hand side represent the contributions of advective transport. The first, second and third terms on the right-hand side of Eq. (1b) represent the effects of forces due to pressure, buoyancy and viscous stress, respectively. Equation (1c) represents the energy conservation equation for small values of Eckert number, which is a standard assumption for the kind of non-Newtonian fluid motion considered here [8–23], and the term on the right-hand side of Eq. (1c) represents diffusion of thermal energy according to the Fourier's law of heat conduction. In Eq. (1b), the Kronecker delta δ_{2i} is employed to ensure that the buoyancy effect only occurs in the vertical

Table 1. The scaling estimates of wall heat flux q_w , characteristic vertical velocity ϑ , thermal boundary layer thicknesses δ_{th} , Nusselt number Nu , effective viscosity μ_{eff} , and effective Rayleigh number Ra_{eff} according to Turan et al. [18]. The function $f_1(Ra, Pr, n)$ represents the ratio of the thicknesses of hydrodynamic and thermal boundary layer [18] and its exact form is not relevant to the current analysis.

Quantity	Scaling relations
Wall heat flux q	$q \sim k\Delta T / \delta_{th} \sim h\Delta T$
Characteristic vertical velocity scale ϑ	$\vartheta \sim \sqrt{g\beta\Delta TL}$
Thermal boundary layer thickness δ_{th}	$\delta_{th} \sim \min \left[L, \frac{1}{f_1(Ra, Pr, n)} \left(\frac{KL(g\beta\Delta TL)^{n/2-1}}{\rho} \right)^{\frac{1}{n+1}} \right]$ $\sim \min \left[L, \frac{1}{f_1(Ra, Pr, n)} \frac{L}{(Ra^{2-n}Pr^{-n})^{\frac{1}{2(n+1)}}} \right]$
Nusselt number Nu	$Nu \sim \frac{hL}{k} \sim \frac{L}{\delta_{th}} \sim \frac{L}{\delta_{th}} f_1 \text{ when } \overline{Nu} > 1$ $\overline{Nu} \sim (Ra_{CWT}^{2-n}Pr^{-n})^{\frac{1}{2(n+1)}} f_1(Ra_{CWT}, Pr, n)$
Effective viscosity $\mu_{eff} \sim K(\vartheta/\delta)^{n-1}$	$\mu_{eff} \sim \rho \left(\frac{K}{\rho} \right)^{\frac{n-1}{n+1}} \frac{(g\beta\Delta TL)^{3(n-1)/2(n+1)}}{L^{(n-1)/(n+1)}}$
Effective Rayleigh number Ra_{eff}	$Ra_{CWT, eff} = \frac{\rho^2 g \beta \Delta T L^3}{\mu_{eff}^2} \frac{\mu_{eff} c_p}{k} \sim Ra^{\frac{5-n}{2n+2}} Pr^{\frac{3-n}{2n+2}}$

direction (i.e., x_2 direction). Here, the rheological behavior is approximated by a power-law model, which leads to the following expression of the viscous stress rate tensor components τ_{ij} [2]:

$$\tau_{ij} = \mu_\alpha e_{ij} = K(e_{kl}e_{kl}/2)^{(n-1)/2} e_{ij} \quad (2)$$

where $e_{ij} = (\partial u_i / \partial x_j + \partial u_j / \partial x_i)$ is the rate of strain tensor, K is the consistency index and n is the power-law index. Accordingly, $\mu_\alpha = K(e_{kl}e_{kl}/2)^{(n-1)/2}$ is the apparent viscosity. It should be noted that the subscripts of ‘ k ’ and ‘ l ’ in e_{kl} of Eq. (2) are dummy indices indicating the summation operation over all possible values of ‘ k ’ and ‘ l ’ according to Einstein’s notation. Considering μ_α , it is evident that μ_α decreases (increases) with increasing shear rate for $n < 1$ ($n > 1$). Therefore, fluids with $n = 1$ represent Newtonian fluids, whereas fluids with $n < 1$ ($n > 1$) represent shear-thinning (shear-thickening) fluids. According to Buckingham’s pi theorem, the Nusselt number (defined as $Nu = hL/k$ where $h = q_w / (T_H - T_C)$ is the local heat transfer coefficient where q_w is the wall heat flux at the bottom wall) can be expressed for the current configuration as $Nu = f(Ra, Pr, n, L/H, \phi)$ where the nominal Rayleigh number Ra , Grashof number Gr and Prandtl number Pr for power-law fluids can be defined as [8–23]:

$$Ra = g\beta\Delta TL^{2n+1} / [\alpha^n (K/\rho)] = Gr.Pr \quad (3a)$$

$$Gr = g\beta\Delta TL^{4n-1} / [\alpha^{2n-2} (K/\rho)^2] \quad (3b)$$

$$Pr = (K/\rho) \alpha^{n-2} L^{2-2n} \quad (3c)$$

where $\Delta T = (T_H - T_C)$ and $\alpha = k/\rho C$ is the thermal diffusivity. It should be noted that in the present study, the aspect ratio H/L is taken to be unity (i.e., $H/L = 1.0$). Turan et al. [18] conducted a detailed scaling analysis to predict the vertical velocity component, boundary layer thickness, mean Nusselt number in the case of natural convection of power-law fluids in enclosed spaces and the summary of that scaling analysis is presented in Table 1. The detailed derivation of the scaling relations is provided elsewhere [18] and thus is not repeated here.

3. Numerical implementation

A finite-volume solver (i.e., ANSYS-Fluent) [62] has been used for solving the governing equations where a second-order upwind scheme (second-order central difference) has been employed for the Discretization of convective (diffusive) terms. The coupling of velocity and pressure

components is achieved using the SIMPLE (Semi-Implicit Method for Pressure-Linked Equations) algorithm [63] and the convergence criteria was set to 10^{-6} for all relative (scaled) residuals. The boundary conditions are: $T = T_H$, $u_1 = u_2 = 0$ at the bottom wall; $T = T_C$, $u_1 = u_2 = 0$ at the sidewalls and $\partial T / \partial y = 0$, $u_1 = u_2 = 0$ at the top wall. The parameters considered are: $Ra = 10^3, 10^4, 10^5$; $n = 0.6, 0.8, 1.0, 1.2, 1.4, 1.6, 1.8$; $Pr = 10, 10^2, 10^3$ and $\phi = 0^\circ, 30^\circ, 45^\circ, 60^\circ$. It should be noted that the values of ϕ allow us to analyze a range of different geometries. The current analysis deals with steady-state laminar natural convection and that is why the highest value of the nominal Rayleigh number Ra for the current analysis is limited to 10^5 . For $Ra < 10^3$, the thermal transport is driven by conduction because the advective transport becomes too weak to affect the heat transfer rate so nominal Rayleigh number values smaller than 10^3 are not considered. The range of the values of n encompasses shear-thinning (i.e., $n < 1$), Newtonian (i.e., $n = 1$) and shear-thickening (i.e., $n > 1$) fluids. For $n = 1.8$, the advective transport becomes too weak to affect thermal transport and the thermal transport takes place almost due to thermal conduction. Thus, the results for $n > 1.8$ for the nominal Rayleigh and Prandtl number values considered here are going to be similar to $n = 1.8$ results and therefore are not considered. The effective Rayleigh number according to the scaling arguments by Turan et al. [8] becomes $Ra_{eff} \sim Ra^{\frac{5-n}{2n+2}} Pr^{\frac{1-n}{2n+2}}$ (where μ_{eff} is the effective viscosity), which suggests that the effective Rayleigh number can be much larger than the nominal Rayleigh number Ra for small values of n for shear-thinning fluids so that a steady-state laminar solution may not exist. Thus, n values smaller than 0.6 are not considered in this analysis. However, the range $0.6 \leq n \leq 1.8$ encompasses several non-Newtonian fluids and is consistent with several previous analyses [3, 4, 8–23]. Non-Newtonian fluids typically exhibit large values of Prandtl number (i.e., $Pr \gg 1$) and can be in the range $10 \leq Pr \leq 10^3$ [1] and therefore Prandtl number values $Pr = 10, 10^2, 10^3$ are considered in this analysis for the purpose of numerical experimentation. The matrix of parameters results in 252 simulations. A mesh independence analysis has been carried out with a non-uniform unstructured triangular mesh of 22,500 cells (shown in Figure 1b) being selected. It should be noted that, as part of the mesh independence analysis, four different mesh sizes were considered (i.e., 50×50 , 100×100 , 150×150 , and 200×200). Moreover, different mesh structures were considered (i.e., non-uniform unstructured triangular mesh, structured triangular mesh, unstructured quadrilateral mesh, and structured quadrilateral mesh). The chosen mesh provides agreement of the mean Nusselt number on the hot wall to within 2% with a mesh of 30,625 cells but with a 26% reduction in computational cost, giving a balance between the accuracy and cost for the parametric investigation. It should be noted that the smallest cell size Δ used across all geometries is $\Delta = 0.005m$. For all the simulations, the maximum and minimum limits of viscosity are taken to be $\mu_{max} = 10^3 \mu_{n=1}$ and $\mu_{min} = 10^{-3} \mu_{n=1}$, respectively where $\mu_{n=1}$ is the viscosity of the Newtonian fluid for the same nominal value of Ra and Pr . It has been found that $\mu_{min} < \mu < \mu_{max}$ are maintained in all the simulations and thus the simulation results remain independent of the choices of μ_{min} and μ_{max} . The currently considered numerical implementations have been compared against benchmarks with the natural convection of Newtonian fluids in a square enclosure (i.e., $\phi = 0^\circ$) with differentially heated sidewalls [27] and natural convection heat transfer in a trapezoidal cavity with differentially heated sides [44]. For both benchmark studies, satisfactory agreements (i.e., typically within 0.5% but, at most, 2% across all benchmark cases) were obtained with Tables 2 and 3 showing the results of the first and second benchmark studies, respectively. The distributions of the nondimensional temperature $\theta = (T - T_C) / (T_H - T_C)$ and nondimensional stream function $\Psi = \psi / \alpha$ for the benchmark problems related to natural convection of Newtonian fluids in a square enclosure with differentially heated sides [27] and natural convection heat transfer in a trapezoidal enclosure with differentially heated vertical sides [44] are shown in Figures 2 and 3, respectively. The spatial distributions of θ and Ψ shown in Figures 2 and 3 are found to be both qualitatively and quantitatively similar to those reported by de Vahl Davis [27] and Moukalled

Table 2. Values of \overline{Nu} , Nu_{\max} , U_{\max} , and V_{\max} at $Ra = 10^3$, 10^4 , 10^5 , and 10^6 for the current numerical implementation compared to the results by de Vahl Davis [27].

Ra	Quantity	Present study	Benchmark [27]	% Difference
10^3	\overline{Nu}	1.118	1.118	0.0000
	Nu_{\max}	1.506	1.505	0.0664
	U_{\max}	3.652	3.649	0.0822
	V_{\max}	3.701	3.697	0.1082
10^4	\overline{Nu}	2.245	2.243	0.0892
	Nu_{\max}	3.532	3.528	0.1134
	U_{\max}	16.203	16.178	0.1545
	V_{\max}	19.670	19.617	0.2702
10^5	\overline{Nu}	4.524	4.519	0.1106
	Nu_{\max}	7.731	7.717	0.1814
	U_{\max}	34.742	34.730	0.0346
	V_{\max}	68.596	68.590	0.0087
10^6	\overline{Nu}	8.839	8.800	0.4432
	Nu_{\max}	17.612	17.925	1.7461
	U_{\max}	64.965	64.63	0.5183
	V_{\max}	220.800	219.360	0.6565

Table 3. Values of \overline{Nu} at $Ra = 10^3$, 10^4 , and 10^5 for the current numerical implementation compared to the results by Moukalled and Darwish [44].

Pr	Quantity	Present study	Benchmark [44]	% Difference
0.7	10^3	0.713	0.715	0.300
	10^4	2.478	2.480	0.063
	10^5	5.474	5.476	0.028
10	10^3	0.717	0.719	0.316
	10^4	2.663	2.666	0.123
	10^5	6.102	6.102	0.007
130	10^3	0.717	0.719	0.306
	10^4	2.667	2.670	0.107
	10^5	6.125	6.125	0.000

and Darwish [44], respectively. Further information related to benchmarking of the numerical schemes used in the current study for power-law fluids is provided elsewhere [18] and interested readers are referred to Turan et al. [18] for this information.

4. Results and discussion

In this section, the effects of Ra , n , Pr , and ϕ on the heat transfer behavior of power-law fluids in a trapezoidal enclosure are explored. The observed effects are accounted for by a correlation for the mean Nusselt number \overline{Nu} across the range of parameters considered in the current study.

4.1. Effects of Rayleigh number Ra

The variations of the mean Nusselt number $\overline{Nu} = L^{-1} \int_0^L Nu \, dx$ for the bottom wall with nominal Rayleigh number Ra across the range of considered power-law index n values for $Pr = 10^2$ and $\phi = 0^\circ$, 30° , 45° , and 60° are shown in Figure 4. The spatial distributions of the local Nusselt number Nu on the bottom wall for $Ra = 10^3$ and 10^5 are exemplarily shown in Figure 5 for $n = 0.6$, 1.0 , and 1.8 , $Pr = 10^2$ and $\phi = 30^\circ$. The trends are qualitatively similar for other values of Ra , Pr , and ϕ and thus are not explicitly shown for the sake of conciseness. It is evident from Figure 5 that the local value of Nusselt number remains high at both ends of the bottom wall and small values of the local Nusselt number is obtained at the middle of the bottom wall. Both ends of hot bottom wall are in the proximity of the cold inclined wall in this configuration and thus the temperature gradient assumes high magnitudes at the ends of the bottom wall and the

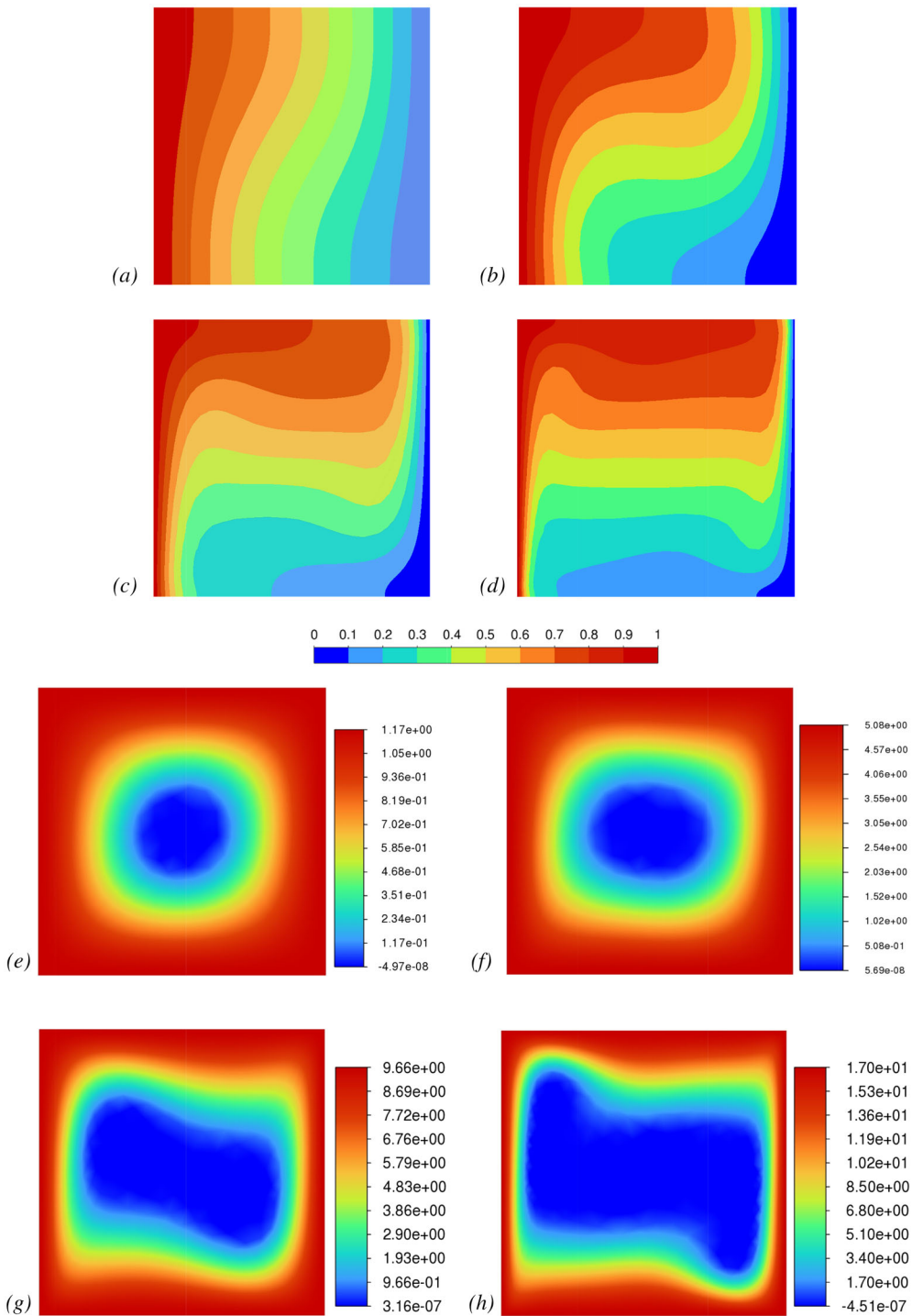


Figure 2. Distributions of nondimensional temperature $\theta = (T - T_C)/(T_H - T_C)$ for (a) $Ra = 10^3$, (b) $Ra = 10^4$, (c) $Ra = 10^5$, and (d) $Ra = 10^6$, and nondimensional stream function $\Psi = \psi/\alpha$ for (d) $Ra = 10^3$, (e) $Ra = 10^4$, (f) $Ra = 10^5$, and (g) $Ra = 10^6$ for the benchmark problem [27].

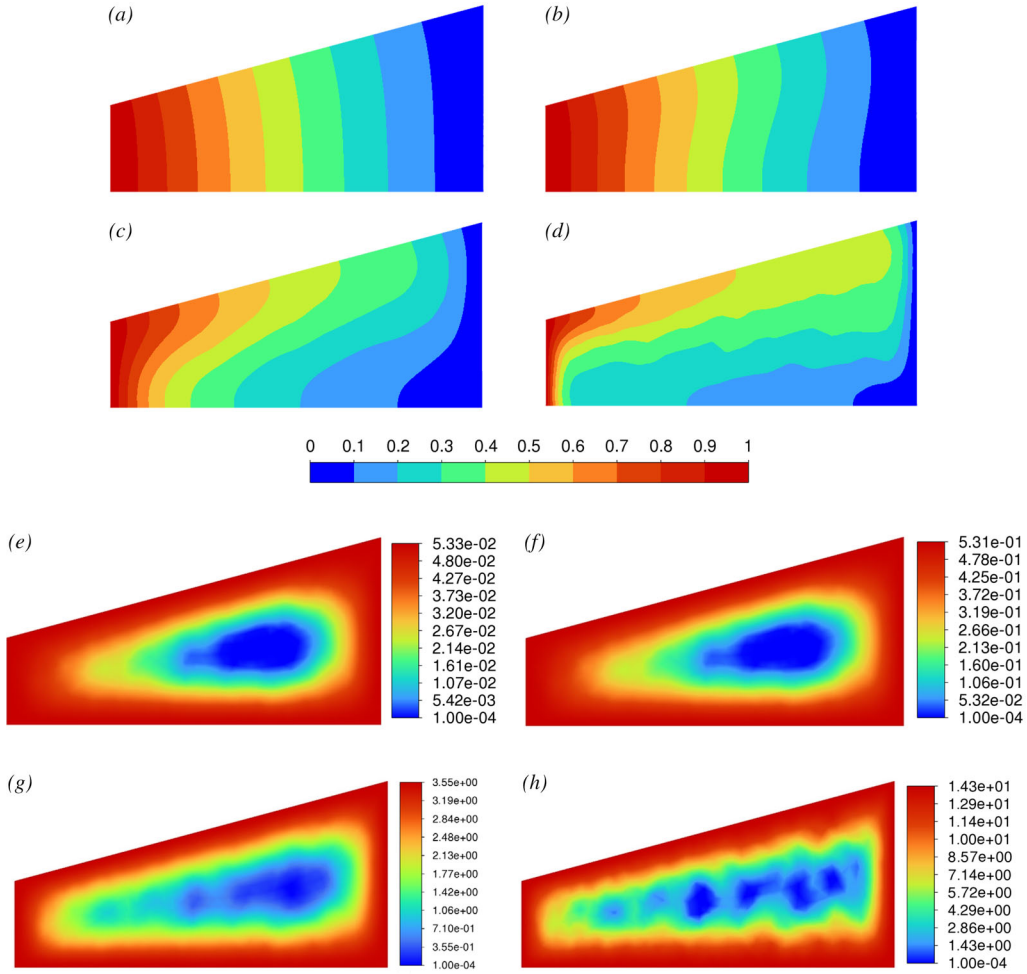


Figure 3. Distributions of nondimensional temperature $\theta = (T - T_C)/(T_H - T_C)$ for (a) $Ra = 10^3$, (b) $Ra = 10^4$, (c) $Ra = 10^5$, and (d) $Ra = 10^6$, and nondimensional stream function $\Psi = \psi/\alpha$ for (e) $Ra = 10^3$, (f) $Ra = 10^4$, (g) $Ra = 10^5$, and (h) $Ra = 10^6$ for the benchmark problem [44].

lowest at the center of the bottom wall because the vertical temperature gradient is the smallest at this point due to this point being the farthest from the cold walls and the horizontal gradient disappears owing to symmetry. The variation of the wall-normal temperature gradient magnitude on the bottom hot wall can further be appreciated from Figure 6 where the distributions of the nondimensional temperature $\theta = (T - T_C)/(T_H - T_C)$ are exemplarily shown for $n = 0.6$, 1.0 and 1.8 at $Ra = 10^3$ and 10^5 in the case of $Pr = 10^2$. It is evident from Figures 4 and 5 that, for a given set of values of Pr and ϕ , the mean Nusselt number \overline{Nu} increases with increasing nominal Rayleigh number Ra . This is consistent with scaling estimates presented in Table 1, which suggests an increasing trend of \overline{Nu} with increasing nominal Rayleigh number Ra . It can be seen from Figure 6 that an increase in Ra for a given value of n leads to a more uniform distribution of θ within the middle of the enclosure and a thinner thermal boundary layer next to the active walls leading to an increase in both local and mean Nusselt numbers (see Figures 4 and 5 and scaling estimate in Table 1). The increase in Nusselt number with increasing Rayleigh number Ra is a result of the strengthening of advective transport. This can be confirmed from the distributions of the nondimensional vertical velocity $U_2 = u_2.L/\alpha$, which are shown exemplarily for $n = 0.6$, 1.0, and 1.8 at $Ra = 10^3$ and 10^5 in the case of $Pr = 10^2$ in Figure 7. It is evident from

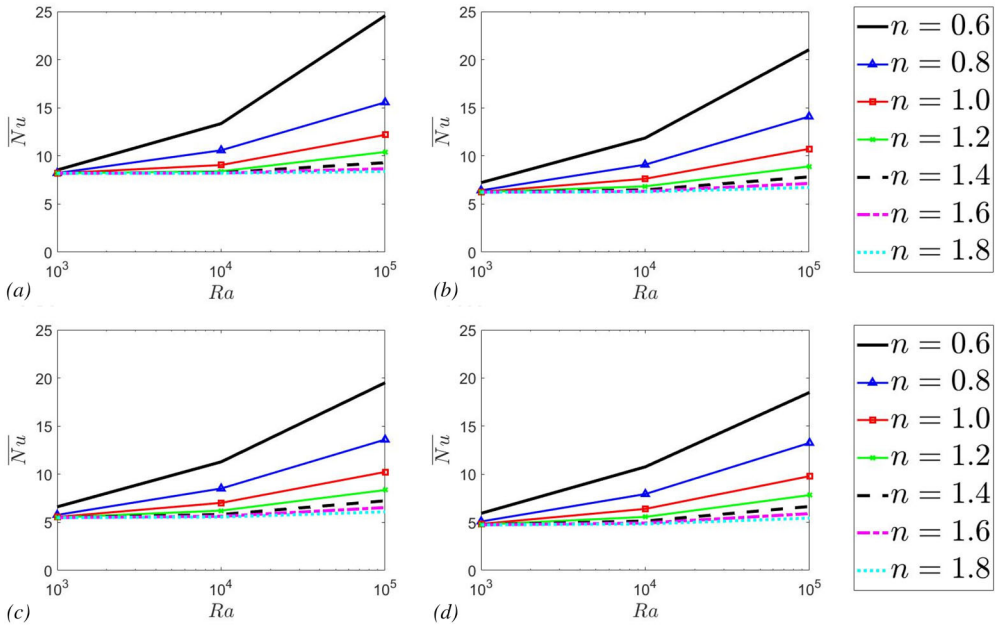


Figure 4. The variations of the mean Nusselt number \overline{Nu} of the bottom wall with Rayleigh number Ra for power-law indices $n = 0.6, 0.8, 1.0, 1.2, 1.4, 1.6$, and 1.8 where Prandtl number $Pr = 10^2$ for inclination angle ϕ of (a) $\phi = 0^\circ$, (b) $\phi = 30^\circ$, (c) $\phi = 45^\circ$, and (d) $\phi = 60^\circ$.

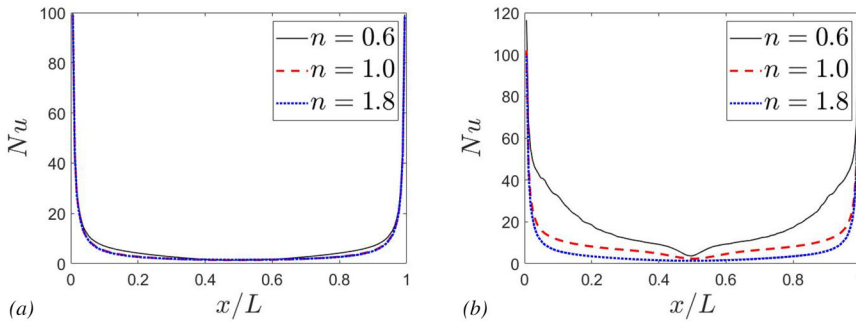


Figure 5. Spatial distributions of local Nusselt Number Nu on the bottom wall for (a) $Ra = 10^3$ and (b) $Ra = 10^5$ on the bottom wall for $n = 0.6, 1.0$, and 1.8 , $Pr = 10^2$ and $\phi = 30^\circ$.

Figure 7 that the magnitude of U_2 increases with increasing Ra , for a given value of n , due to strengthening of buoyancy forces relative to the viscous forces, which in turn leads to the augmentation of advective transport. The relative strength of the buoyancy force increases with increasing Ra , and therefore, advective transport plays an increasingly significant role in the overall heat transfer relative to thermal diffusion, and accordingly, the mean Nusselt number \overline{Nu} increases.

4.2. Effects of power-law index n

It can be seen from Figures 4 and 5 that the increases in both mean and local Nusselt numbers with increasing Ra occur across all values of power-law index n considered. Furthermore, \overline{Nu} increases with decreasing n for a given value of Ra . The variations of the mean Nusselt number \overline{Nu} with power-law index n across the range for $\phi = 0^\circ, 30^\circ, 45^\circ$, and 60° where $Pr = 10^2$ for

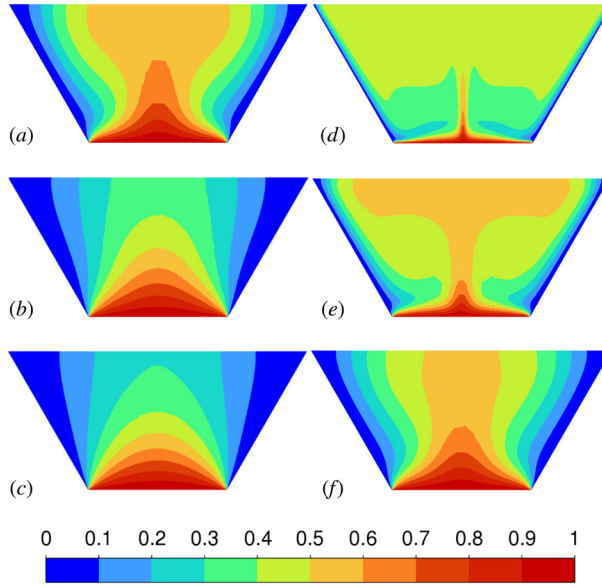


Figure 6. The distributions of nondimensional temperature $\theta = (T - T_C)/(T_H - T_C)$ for Prandtl number $Pr = 10^2$ and inclination angle $\phi = 30^\circ$ for (a) $n = 0.6$, $Ra = 10^3$, (b) $n = 1.0$, $Ra = 10^3$, (c) $n = 1.8$, $Ra = 10^3$, (d) $n = 0.6$, $Ra = 10^5$, (e) $n = 1.0$, $Ra = 10^5$, and (f) $n = 1.8$, $Ra = 10^5$.

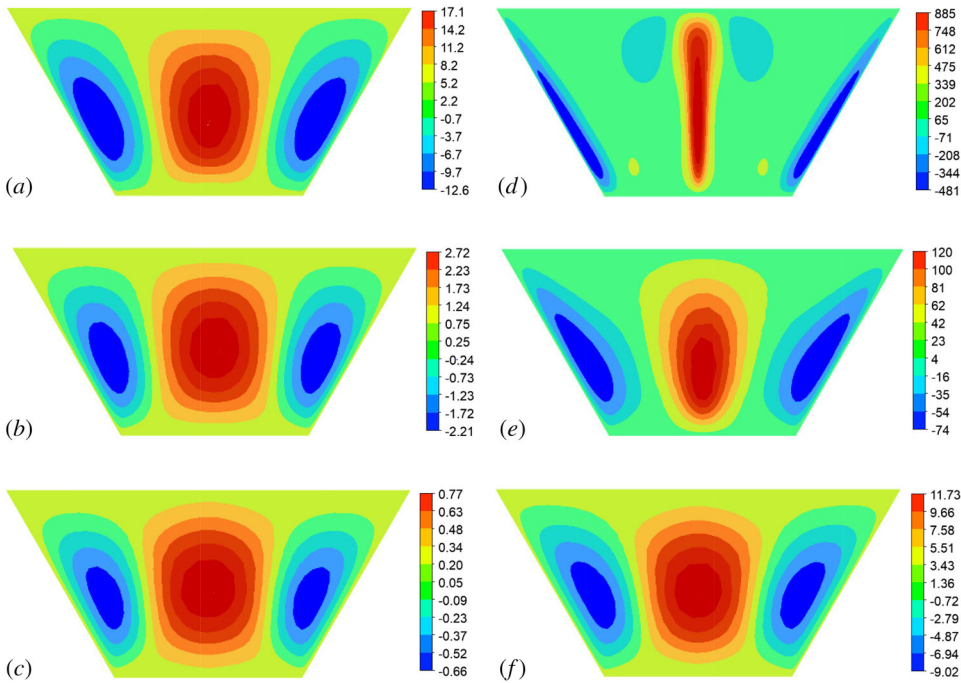


Figure 7. The distributions of nondimensional vertical velocity $U_2 = u_{2,L}/\alpha$ for Prandtl $Pr = 10^2$ and inclination angle $\phi = 30^\circ$ for (a) $n = 0.6$, $Ra = 10^3$, (b) $n = 1.0$, $Ra = 10^3$, (c) $n = 1.8$, $Ra = 10^3$, (d) $n = 0.6$, $Ra = 10^5$, (e) $n = 1.0$, $Ra = 10^5$, and (f) $n = 1.8$, $Ra = 10^5$. It should be noted that the colourbar axis are different in each subfigure due to the wide variations in magnitude of U_2 for the considered cases.

$Ra = 10^3$, 10^4 , and 10^5 are shown in Figures 8a–8c, respectively. It is evident from Figures 8a–8c that, for a given set of values of Ra , Pr , and ϕ , the mean Nusselt number \overline{Nu} decreases with increasing power-law index n , which is also consistent with scaling estimates presented in

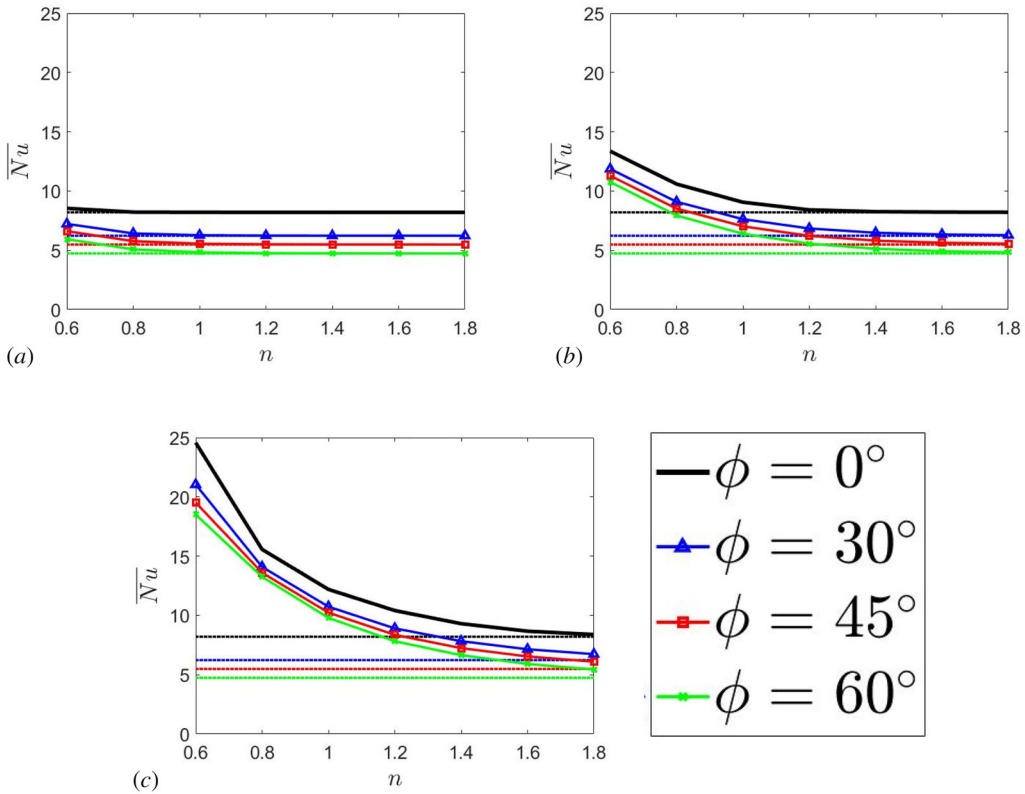


Figure 8. The variations of the mean Nusselt number \overline{Nu} of the bottom wall with power-law index n across the range for inclination angles $\phi = 0^\circ$, 30° , 45° , and 60° where Prandtl number $Pr = 10^2$ for Rayleigh number Ra of (a) $Ra = 10^3$, (b) $Ra = 10^4$, and (c) $Ra = 10^5$. The dashed lines indicate the values of the mean Nusselt number \overline{Nu} for pure conduction for the corresponding inclination angle ϕ .

Table 1. Furthermore, the rate of reduction of \overline{Nu} with increasing n is relatively high for shear-thinning fluids (i.e., $0.6 < n < 1$). As n increases from $n = 1.0$ to $n = 1.8$, the rate of reduction in \overline{Nu} becomes gradual until settling toward a Nusselt number value which is obtained for pure conductive transport for large values of n . The increase in the magnitude of the local Nusselt number Nu with decreasing n for a given value of nominal Rayleigh number can also be seen from Figure 4 but this trend is particularly strong for high values of Ra . The variations of U_2 and θ along the vertical midplane are exemplarily shown for $n = 0.6$, 1.0 , and 1.8 at $Ra = 10^3$ and 10^5 in the case of $Pr = 10^2$ in Figure 9. It can be appreciated from θ variations with y/L in Figures 9a–9c that the temperature gradient at the heated bottom wall (i.e., $y/L = 0$) increases with decreasing n for $Ra = 10^5$, which is reflected in marked increases in Nu and \overline{Nu} for this nominal Rayleigh number (see Figures 4 and 8). This is also consistent with the scaling analysis predictions of the thermal boundary layer thickness and Nusselt number presented in Table 1. Moreover, θ variations with y/L in Figures 9a–9c indicate that the vertical temperature gradients at the heated bottom wall (i.e., $y/L = 0$) are comparable for different values of n for $Ra = 10^3$, which are reflected in the similar values of local and mean Nusselt numbers (see Figures 4 and 8). It can further be seen from Figures 9d–9f that the magnitude of U_2 increases with decreasing n for a given value of Ra along with marked increases in U_2 magnitude with increasing Ra for a given value of n . This demonstrates strengthening of advective transport with decreasing n due to the weakening of viscous resistance and increasing Ra due to strengthening of buoyancy effects. This is also reflected in the decreases in U_2 magnitude with increasing n , for a given value of

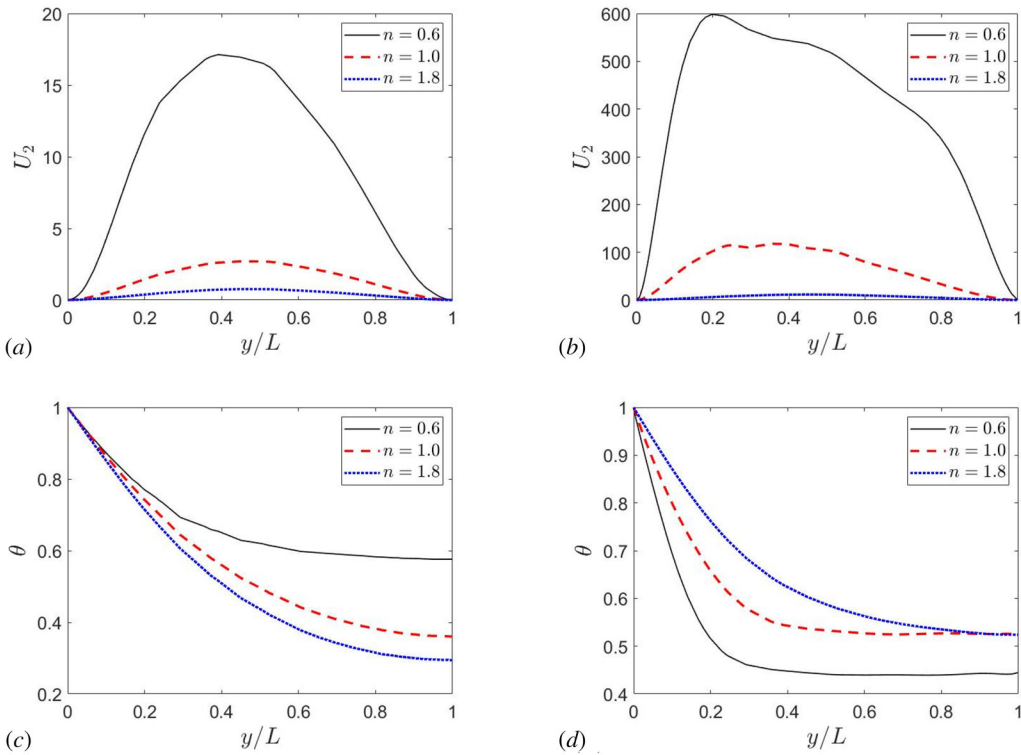


Figure 9. Variations of U_2 at (a) $Ra = 10^3$ and (b) $Ra = 10^5$ and θ at (c) $Ra = 10^3$ and (d) $Ra = 10^5$ along the vertical midplane for $n = 0.6, 1.0$, and 1.8 in the case of $Pr = 10^2$.

Ra , in Figure 6 due to the strengthening of viscous forces due to the shear-thickening effects, leading to greater contribution of conduction to the overall thermal transport. Therefore, a decrease in n for a given value of Ra leads to a more uniform distribution of θ at the core of the enclosure and thinner thermal boundary layer, as evident from Figure 6, which leads to a higher value of local and mean Nusselt numbers (see Figures 4 and 8).

4.3. Effects of Prandtl number Pr

The variations of the mean Nusselt number \overline{Nu} with Prandtl number Pr across the range of considered power index n values for $Ra = 10^5$ and $\phi = 0^\circ, 30^\circ, 45^\circ$, and 60° are exemplarily shown in Figure 10 and the same qualitative behavior was observed for other values of Ra . It can be seen from Figure 10 that, for a given set of values of Ra , n , and ϕ , \overline{Nu} does not vary significantly with increasing Pr . This observation is consistent with previous analyses of different configurations [8–15, 19–23]. However, the influence of Pr was slightly noticeable in the mean Nusselt number for shear thinning fluids with small values of n (i.e., $n = 0.6$). It should be noted that the thermal boundary layer δ_{th} is expected to be thinner than the hydrodynamic boundary layer δ (i.e., $\delta \gg \delta_{th}$) when $Pr \gg 1$. Non-Newtonian fluids typically have Prandtl numbers much larger than unity (i.e., $Pr \gg 1$). The relative balances of inertial and viscous forces govern the transport behavior within the hydrodynamic boundary layer outside the thermal boundary layer [64]. Thus, a modification in Prandtl number for $Pr \gg 1$ acts to modify the relative balance between viscous and inertial forces in natural convection for a major part of the hydrodynamic boundary layer, whereas the thermal transport within the thermal boundary layer is marginally

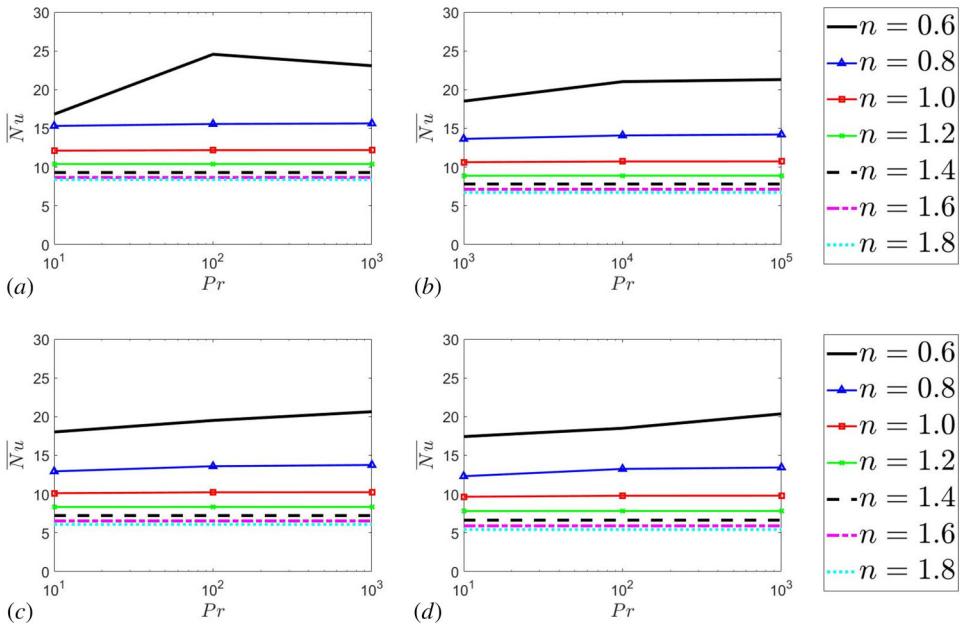


Figure 10. The variations of the mean Nusselt number \overline{Nu} of the bottom wall with nominal Prandtl number Pr for different values of power-law index n at Rayleigh number $Ra = 10^5$ for inclination angle ϕ of (a) $\phi = 0^\circ$, (b) $\phi = 30^\circ$, (c) $\phi = 45^\circ$, and (d) $\phi = 60^\circ$.

affected [64]. As a result, the mean Nusselt number \overline{Nu} does not demonstrate any significant Prandtl number Pr dependence where $Pr \gg 1$. The hydrodynamic boundary layer is, for the power-law indices considered here, the thinnest for $n = 0.6$ and, therefore, δ assumes a value closer to δ_{th} in this case where the heat transfer is slightly affected by the competition between inertial and viscous forces.

4.4. Effects of angle of inclination of cooled side walls ϕ

The variations of the mean Nusselt number \overline{Nu} with inclination angle ϕ for different values of n for $Pr = 10^2$ are exemplarily shown in Figures 11a–11c for $Ra = 10^3$, 10^4 , and 10^5 , respectively. It is evident from Figures 11a–11c that \overline{Nu} decreases with increasing ϕ which is due to the walls at temperature T_C (i.e., cold walls, inclined to the vertical) becoming longer leading to greater area for losing heat from the cavity and, therefore, a smaller amount of heat flux is needed for higher values of ϕ to maintain the same $\Delta T = (T_H - T_C)$. However, the observed reduction in \overline{Nu} with ϕ is small and, furthermore, the variations of \overline{Nu} with ϕ have mostly similar gradients for all power-law indices, and the effect of ϕ on \overline{Nu} is relatively weak compared to its Ra and n dependences.

4.5. Mean Nusselt number \overline{Nu} correlation

A correlation for the mean Nusselt number \overline{Nu} is proposed here based upon the scaling arguments of Turan et al. [18] in the following manner:

$$\overline{Nu} = C_1 \cdot (Ra^{2-n}/Pr^n)^{1/(2n+2)} \cdot n^{C_2} \text{ for } C_1 \cdot (Ra^{2-n}/Pr^n)^{1/(2n+2)} \cdot n^{C_2} > 1 \quad (4a)$$

$$\overline{Nu} = 1.0 \text{ for } C_1 \cdot (Ra^{2-n}/Pr^n)^{1/(2n+2)} \cdot n^{C_2} \leq 1 \quad (4b)$$

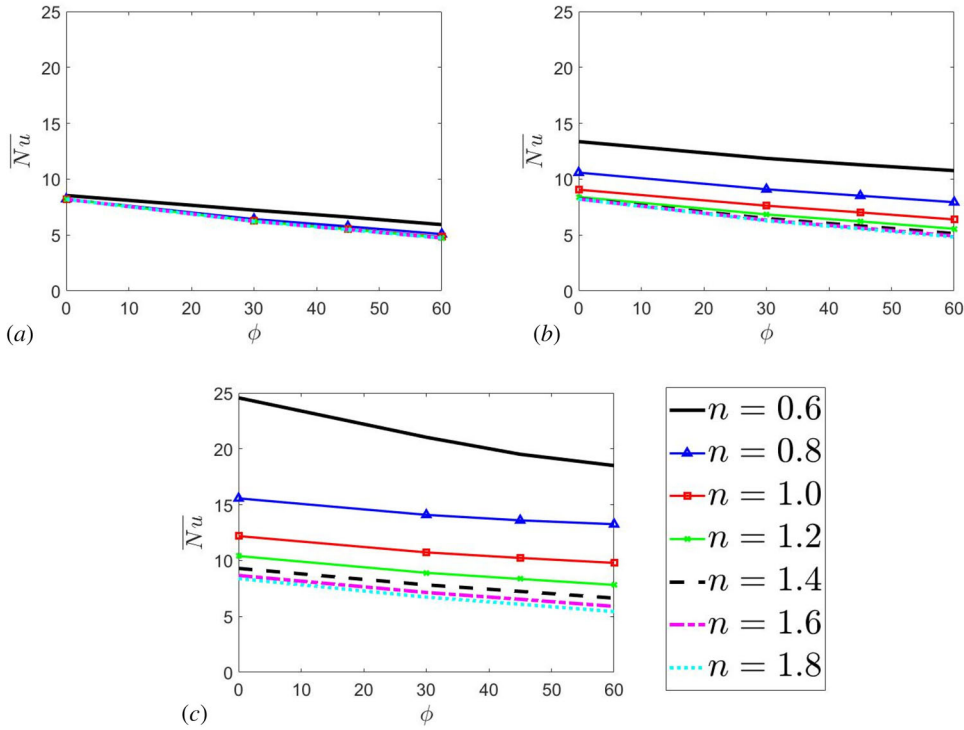


Figure 11. The variations of the mean Nusselt number \overline{Nu} of the bottom wall with inclination angle ϕ for power-law indices $n = 0.6, 0.8, 1.0, 1.2, 1.4, 1.6$, and 1.8 where Prandtl number $Pr = 10^2$ for Rayleigh number Ra of (a) $Ra = 10^3$, (b) $Ra = 10^4$, and (c) $Ra = 10^5$.

where C_1 and C_2 are model parameters with $C_1 = 2.0(1.3^{-\phi[rad]})$ and $C_2 = 0.4[Ra^{0.18}]$ for $n < 1$, and $C_1 = 1.56(Ra^{-0.18})(Pr^{0.5})(1.5^{-\phi[rad]})$ and $C_2 = 1.93(Ra^{0.07})(1.025^{-\phi[rad]})$ for $n \geq 1$. It is evident from Figures 12a–12d that Eq. (4) adequately captures the qualitative and quantitative behavior of the mean Nusselt number \overline{Nu} across the range of Rayleigh numbers Ra , power-law index n , Prandtl number Pr , and inclination angle ϕ with a coefficient of determination R^2 greater than 0.97 (i.e., $R^2 > 0.97$).

5. Conclusions

Steady-state laminar natural convection of power-law fluids in 2-D trapezoidal enclosures with a heated bottom wall, adiabatic top and cooled inclined sidewalls has been analyzed based on numerical simulations for the very first time for a range of different values of nominal Rayleigh number Ra (i.e., $Ra = 10^3, 10^4$, and 10^5), Prandtl number Pr (i.e., $Pr = 10^1, 10^2$, and 10^3), power-law index n (i.e., $n = 0.6, 0.8, 1.0, 1.2, 1.4, 1.6$, and 1.8) and ϕ (i.e., $\phi = 0^\circ, 30^\circ, 45^\circ$ and 60°). The main findings of this study are as follows:

- The mean Nusselt number \overline{Nu} has been observed to increase with increasing Ra (up to a 187% increase for $n = 0.6$ and up to 2.3% increase for $n = 1.8$ between $Ra = 10^3$ and 10^5) due to the strengthening of advective transport contribution to the overall heat transfer. Moreover, the value of \overline{Nu} was found to increase with decreasing n (up to a 4.1% increase for $Ra = 10^3$ and up to 193% increase for $Ra = 10^5$ between $n = 0.6$ and 1.8) due to the strengthening of buoyancy forces in comparison to the viscous forces in the shear-thinning fluids.

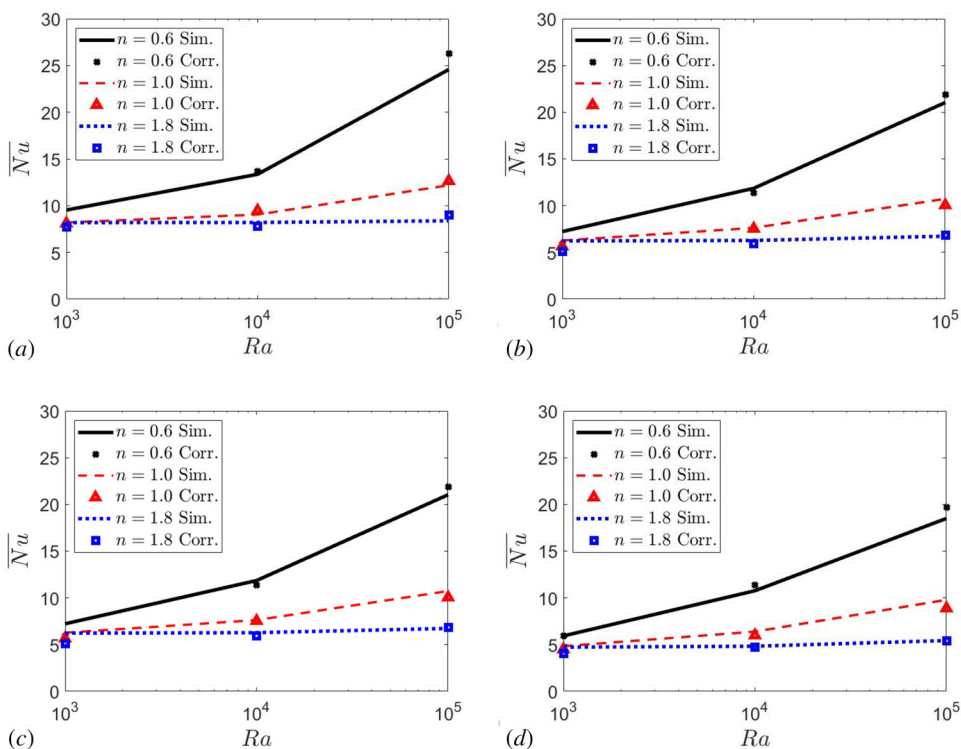


Figure 12. The variations of mean Nusselt number \overline{Nu} of the bottom wall with Rayleigh number Ra for power-law indices $n = 0.6, 1.0$, and 1.8 where Prandtl number $Pr = 10^2$ from the simulations (i.e. Sim.) with the values of the Eq. (4) correlation (i.e. Corr.) values for inclination angle ϕ of (a) $\phi = 0^\circ$, (b) $\phi = 30^\circ$, (c) $\phi = 45^\circ$, and (d) $\phi = 60^\circ$.

- However, an increase in the sidewall inclination ϕ leads to a decrease in \overline{Nu} (approximately 44% decrease for $Ra = 10^3$ across values of n and up to 33% decrease for $Ra = 10^5$ across values of n) due to an increase in the length of the cooled walls, leading to greater area for losing heat from the enclosure and therefore a smaller amount of heat flux is needed for higher values of ϕ to maintain the same temperature difference ΔT .
- It has been found that \overline{Nu} does not vary significantly for the values of Pr considered.

Detailed physical explanations have been provided for the aforementioned trends. Furthermore, a new correlation for \overline{Nu} has been proposed for natural convection in trapezoidal enclosures with a heated bottom wall, cooled inclined sidewalls, and an adiabatic top wall accounting for the range of Ra , n , Pr , and ϕ considered here. The correlation was shown to satisfactorily predict the corresponding \overline{Nu} values obtained from the simulations. This information can be important for engineering applications ranging from electronic cooling to food and chemical processing to name a few.

Disclosure statement

We have no competing interests.

Ethics statement

This work did not involve any active collection of human data.

ORCID

N. Chakraborty  <http://orcid.org/0000-0003-1690-2036>

References

- [1] M. Darbouli, C. Métivier, S. Leclerc, C. Nouar, M. Bouteera, and D. Stemmelen, "Natural convection in shear-thinning fluids: experimental investigations by MRI," *Int. J. Heat Mass Transf.*, vol. 95, pp. 742–754, Apr. 2016. DOI: [10.1016/j.ijheatmasstransfer.2015.12.056](https://doi.org/10.1016/j.ijheatmasstransfer.2015.12.056).
- [2] H. Ozoe and S. W. Churchill, "Hydrodynamic stability and natural convection in Ostwald-De Waele and Ellis fluids: the development of a numerical solution," *AIChE J.*, vol. 18, no. 6, pp. 1196–1207, Nov. 1972. DOI: [10.1002/aic.690180617](https://doi.org/10.1002/aic.690180617).
- [3] M. Lamsaadi, M. Naïmi, and M. Hasnaoui, "Natural convection of non-Newtonian power law fluids in a shallow horizontal rectangular cavity uniformly heated from below," *Heat Mass Transf.*, vol. 41, no. 3, pp. 239–249, Jan. 2005. DOI: [10.1007/s00231-004-0530-8](https://doi.org/10.1007/s00231-004-0530-8).
- [4] M. Lamsaadi, M. Naïmi, M. Hasnaoui, and M. Mamou, "Natural convection in a vertical rectangular cavity filled with a non-Newtonian power law fluid and subjected to a horizontal temperature gradient," *Numer. Heat Transf. A*, vol. 49, no. 10, pp. 969–990, Sep. 2006. DOI: [10.1080/10407780500324988](https://doi.org/10.1080/10407780500324988).
- [5] Z. Alloui, N. Ben Khelifa, H. Beji, P. Vasseur, and A. Guizani, "The onset of convection of power-law fluids in a shallow cavity heated from below by a constant heat flux," *J. Non-Newt. Fluid Mech.*, vol. 196, pp. 70–82, Jun. 2013. DOI: [10.1016/j.jnnfm.2013.01.008](https://doi.org/10.1016/j.jnnfm.2013.01.008).
- [6] M. Ohta, M. Ohta, M. Akiyoshi, and E. Obata, "A numerical study on natural convective heat transfer of pseudo-plastic fluids in a square cavity," *Numer. Heat Transf. A*, vol. 41, no. 4, pp. 357–372, Mar. 2002. DOI: [10.1080/104077802317261218](https://doi.org/10.1080/104077802317261218).
- [7] H. Inaba, C. Daib, and A. Horibe, "Natural convection heat transfer of micro-emulsion phase-change materials slurry in rectangular cavities heated from below and cooled from above," *Int. J. Heat Mass Trans.*, vol. 46, no. 23, pp. 4427–4438, 2003. DOI: [10.1016/S0017-9310\(03\)00289-8](https://doi.org/10.1016/S0017-9310(03)00289-8).
- [8] O. Turan, J. Lai, N. Chakraborty, and R. J. Poole, "Laminar natural convection of power-law fluids in square enclosures heated from below subjected to constant wall heat fluxes," *J. Non-Newt. Fluid Mech.*, vol. 199, pp. 80–95, Sep. 2013. DOI: [10.1016/j.jnnfm.2013.06.002](https://doi.org/10.1016/j.jnnfm.2013.06.002).
- [9] O. Turan, F. Fotso-Choupe, J. Lai, R. J. Poole, and N. Chakraborty, "Boundary condition effects on laminar natural convection of power-law fluids in a square enclosure heated from below with differentially heated horizontal walls," *Ind. Eng. Chem. Res.*, vol. 53, no. 1, pp. 456–473, 2014. DOI: [10.1021/ie4023447](https://doi.org/10.1021/ie4023447).
- [10] S. Yigit, R. J. Poole, and N. Chakraborty, "Effects of aspect ratio effects on laminar Rayleigh-Bénard convection of power-law fluids in rectangular enclosures: a numerical investigation," *Int. J. Heat Mass Trans.*, vol. 91, pp. 1292–1307, Dec. 2015. DOI: [10.1016/j.ijheatmasstransfer.2015.08.032](https://doi.org/10.1016/j.ijheatmasstransfer.2015.08.032).
- [11] S. Yigit, C. McRoberts, and N. Chakraborty, "Numerical investigation of laminar Rayleigh-Bénard convection of power-law fluids in square cross-sectional cylindrical annular enclosures," *Int. Commun. Heat Mass Transf.*, vol. 78, pp. 112–120, Nov. 2016. DOI: [10.1016/j.icheatmasstransfer.2016.08.025](https://doi.org/10.1016/j.icheatmasstransfer.2016.08.025).
- [12] S. Yigit and N. Chakraborty, "Rayleigh-Bénard power-law fluid convection in rectangular enclosures," *AIAA J. Thermophys. Heat Transf.*, vol. 31, no. 4, pp. 805–816, Apr. 2017. DOI: [10.2514/1.T5108](https://doi.org/10.2514/1.T5108).
- [13] S. Yigit and N. Chakraborty, "Numerical investigation of aspect ratio influences on Rayleigh-Bénard convection of power-law fluids in vertical cylindrical annuli," *Therm. Sci. Eng. Prog.*, vol. 9, pp. 185–199, Mar. 2019. DOI: [10.1016/j.tsep.2018.10.007](https://doi.org/10.1016/j.tsep.2018.10.007).
- [14] S. Yigit, M. Battu, O. Turan, and N. Chakraborty, "Free convection of power-law fluids in enclosures with partially heating from bottom and symmetrical cooling from sides," *Int. J. Heat Mass Transf.*, vol. 145, pp. 118782, Dec. 2019. DOI: [10.1016/j.ijheatmasstransfer.2019.118782](https://doi.org/10.1016/j.ijheatmasstransfer.2019.118782).
- [15] S. Yigit, F. Brauer, N. Chakraborty, and M. Klein, "Comparison of two and three-dimensional Rayleigh-Bénard convection of power-law fluids in cylindrical and annular enclosures," *Int. J. Heat Transf.*, vol. 160, pp. 120211, 2020. DOI: [10.1016/j.ijheatmasstransfer.2020.120211](https://doi.org/10.1016/j.ijheatmasstransfer.2020.120211).
- [16] G. B. Kim, J. M. Hyun, and H. S. Kwak, "Transient buoyant convection of a power law non-Newtonian fluid in an enclosure," *Int. J. Heat Mass Transf.*, vol. 46, no. 19, pp. 3605–3617, Sep. 2003. DOI: [10.1016/S0017-9310\(03\)00149-2](https://doi.org/10.1016/S0017-9310(03)00149-2).
- [17] M. Lamsaadi, M. Naïmi, and M. Hasnaoui, "Natural convection heat transfer in shallow horizontal rectangular enclosures uniformly heated from the side and filled with non-Newtonian power law fluids," *Energy Convers. Manag.*, vol. 47, no. 15–16, pp. 2535–2551, Sep. 2006. DOI: [10.1016/j.enconman.2005.10.028](https://doi.org/10.1016/j.enconman.2005.10.028).
- [18] O. Turan, A. Sachdeva, N. Chakraborty, and R. J. Poole, "Laminar natural convection of power-law fluids in a square enclosure with differentially heated side walls subjected to constant temperatures," *J. Non-Newt. Fluid Mech.*, vol. 166, no. 17–18, pp. 1049–1063, Sep. 2011. DOI: [10.1016/j.jnnfm.2011.06.003](https://doi.org/10.1016/j.jnnfm.2011.06.003).

- [19] O. Turan, A. Sachdeva, R. J. Poole, and N. Chakraborty, "Laminar natural convection of power-law fluids in a square enclosure with differentially heated side walls subjected to constant wall heat flux," *J. Heat Transf.*, vol. 134, no. 12, pp. 122504, Dec. 2012. DOI: [10.1115/1.4007123](https://doi.org/10.1115/1.4007123).
- [20] O. Turan, A. Sachdeva, R. J. Poole and N. Chakraborty, "Aspect ratio and boundary conditions effects on laminar natural convection of power-law fluids in a rectangular enclosure with differentially heated side walls," *Int. J. Heat Mass Transf.*, vol. 60, pp. 722–738, May 2013. DOI: [10.1016/j.ijheatmasstransfer.2013.01.017](https://doi.org/10.1016/j.ijheatmasstransfer.2013.01.017).
- [21] S. Yigit, J. Ford, R. J. Poole, and N. Chakraborty, "Numerical Investigation of boundary condition effects on natural convection of power-law fluids in square cross-section annular cylindrical spaces with differentially heated vertical wall: effects of different boundary condition," *Comput. Therm. Sci.*, vol. 7, no. 3, pp. 261–282, Jan. 2015. DOI: [10.1615/ComputThermalScien.2015014174](https://doi.org/10.1615/ComputThermalScien.2015014174).
- [22] S. Yigit, T. Graham, R. J. Poole, and N. Chakraborty, "Numerical investigation of steady-state laminar natural convection of power-law fluids in annular cylindrical space with square cross-section for differentially heated vertical walls: a computational analysis," *Int. J. Numer. Heat Fluid Flow*, vol. 26, no. 1, pp. 85–107, Jan. 2016. DOI: [10.1108/HFF-01-2015-0030](https://doi.org/10.1108/HFF-01-2015-0030).
- [23] S. Yigit and N. Chakraborty, "Influences of aspect ratio on natural convection of power law fluids in cylindrical annular space with differentially heated vertical walls," *Therm. Sci. Eng. Prog.*, vol. 2, pp. 151–164, Jun. 2017. DOI: [10.1016/j.tsep.2017.05.008](https://doi.org/10.1016/j.tsep.2017.05.008).
- [24] I. Catton, P. S. Ayyaswamy, and R. M. Clever, "Natural convection flow in a finite, rectangular slot arbitrarily oriented with respect to the gravity vector," *Int. J. Heat Mass Transf.*, vol. 17, no. 2, pp. 173–184, Feb. 1974. DOI: [10.1016/0017-9310\(74\)90079-9](https://doi.org/10.1016/0017-9310(74)90079-9).
- [25] S. Ostrach, "Natural convection in enclosure," *J. Heat Transf.*, vol. 110, no. 4b, pp. 1175–1190, Nov. 1988. DOI: [10.1115/1.3250619](https://doi.org/10.1115/1.3250619).
- [26] T. Fusegi, J. M. Hyun, K. Kumahara, and B. Farouk, "A numerical study of three-dimensional natural convection in a differentially heated cubical enclosure," *Int. J. Heat Mass Transf.*, vol. 34, no. 6, pp. 1543–1557, Jun. 1991. DOI: [10.1016/0017-9310\(91\)90295-P](https://doi.org/10.1016/0017-9310(91)90295-P).
- [27] G. de Vahl Davis, "Natural convection of air in a square cavity: a benchmark solution," *Int. J. Numer. Meth. Fluids*, vol. 3, no. 3, pp. 249–264, May/Jun. 1983. DOI: [10.1002/fld.1650030305](https://doi.org/10.1002/fld.1650030305).
- [28] E. Bodenschatz, W. Pesch, and G. Ahlers, "Recent developments in Rayleigh–Bénard convection," *Annu. Rev. Fluid Mech.*, vol. 32, no. 1, pp. 709–778, Jan. 2000. DOI: [10.1146/annurev.fluid.32.1.709](https://doi.org/10.1146/annurev.fluid.32.1.709).
- [29] A. A. Ganguli, A. B. Pandit, and J. B. Joshi, "CFD simulation of heat transfer in a two-dimensional vertical enclosure," *Chem. Eng. Res. Design*, vol. 87, no. 5, pp. 711–727, May 2009. DOI: [10.1016/j.cherd.2008.11.005](https://doi.org/10.1016/j.cherd.2008.11.005).
- [30] O. Turan, R. J. Poole, and N. Chakraborty, "Influences of boundary conditions on laminar natural convection in rectangular enclosures with differentially heated side walls," *Int. J. Heat Fluid Flow*, vol. 33, no. 1, pp. 131–146, Feb. 2012. DOI: [10.1016/j.ijheatfluidflow.2011.10.009](https://doi.org/10.1016/j.ijheatfluidflow.2011.10.009).
- [31] M. S. Aghighi, A. Ammar, H. Masoumi, and A. Lanjani, "Rayleigh–Bénard convection of a viscoplastic liquid in a trapezoidal enclosure," *Int. J. Mech. Sci.*, vol. 180, pp. 105630, Aug. 2020. DOI: [10.1016/j.jimecs.2020.105630](https://doi.org/10.1016/j.jimecs.2020.105630).
- [32] A. K. Hussein, et al., "Three-dimensional unsteady natural convection and entropy generation in an inclined cubical trapezoidal cavity with an isothermal bottom wall," *Alex. Eng. J.*, vol. 55, no. 2, pp. 741–755, Jun. 2016. DOI: [10.1016/j.aej.2016.01.004](https://doi.org/10.1016/j.aej.2016.01.004).
- [33] L. Iyican, L. C. Witte, and Y. Bayazitoglu, "An experimental study of natural convection in trapezoidal enclosures," *J. Heat Transf.*, vol. 102, no. 4, pp. 648–653, Nov. 1980. DOI: [10.1115/1.3244366](https://doi.org/10.1115/1.3244366).
- [34] S. W. Lam, R. Gani, and J. G. Simons, "Experimental and numerical Studies of natural convection in trapezoidal cavities," *J. Heat Transf.*, vol. 111, no. 2, pp. 372–377, May 1989. DOI: [10.1115/1.3250687](https://doi.org/10.1115/1.3250687).
- [35] Y. E. Karyakin, "Transient natural convection in prismatic enclosures of arbitrary cross-section," *Int. J. Heat Mass Transf.*, vol. 32, no. 6, pp. 1095–1103, Jun. 1989. DOI: [10.1016/0017-9310\(89\)90009-4](https://doi.org/10.1016/0017-9310(89)90009-4).
- [36] T. S. Lee, "Numerical experiments with fluid convection in tilted nonrectangular enclosures," *Numer. Heat Transf. A*, vol. 19, no. 4, pp. 487–499, 1991. DOI: [10.1080/10407789108944861](https://doi.org/10.1080/10407789108944861).
- [37] T. S. Lee, "Computational and experimental studies of convective fluid motion and heat transfer in inclined non-rectangular enclosures," *Int. J. Heat Fluid Flow*, vol. 5, no. 1, pp. 29–36, 1984. Mar DOI: [10.1016/0142-727X\(84\)90009-2](https://doi.org/10.1016/0142-727X(84)90009-2).
- [38] M. Peric, "Natural convection in trapezoidal cavities," *Numer. Heat Transf. A*, vol. 24, no. 2, pp. 213–219, 1993. DOI: [10.1080/10407789308902614](https://doi.org/10.1080/10407789308902614).
- [39] H. Sadat and P. Salagnac, "Further results for laminar natural convection in a two-dimensional trapezoidal enclosure," *Numer. Heat Transf. A*, vol. 27, no. 4, pp. 451–459, 1995. DOI: [10.1080/10407789508913711](https://doi.org/10.1080/10407789508913711).
- [40] R. A. Kuypers and C. J. Hoogendoorn, "Laminar natural convection flow in trapezoidal enclosures," *Numer. Heat Transf. A*, vol. 28, no. 1, pp. 55–67, 1995. DOI: [10.1080/10407789508913732](https://doi.org/10.1080/10407789508913732).
- [41] F. Moukalled and S. Acharya, "Buoyancy-induced heat transfer in partially divided trapezoidal cavities," *Numer. Heat Transf. A*, vol. 32, no. 8, pp. 787–810, 1997. DOI: [10.1080/10407789708913918](https://doi.org/10.1080/10407789708913918).

- [42] F. Moukalled and S. Acharya, "Natural convection in trapezoidal cavities with baffles mounted on the upper inclined surfaces," *Numer. Heat Transf. A*, vol. 37, no. 6, pp. 545–565, May 2000. DOI: [10.1080/104077800274082](https://doi.org/10.1080/104077800274082).
- [43] F. Moukalled and S. Acharya, "Natural convection in a trapezoidal enclosure with offset baffles," *AIAA J. Thermophys. Heat Transf.*, vol. 15, no. 2, pp. 212–218, Apr. 2001. DOI: [10.2514/2.6596](https://doi.org/10.2514/2.6596).
- [44] F. Moukalled and M. Darwish, "Natural convection in partitioned trapezoidal cavity heated from the side," *Numer. Heat Transf. A*, vol. 43, no. 5, pp. 543–563, Nov. 2003. DOI: [10.1080/10407780307313](https://doi.org/10.1080/10407780307313).
- [45] A. da Silva, É. Fontana, V. C. Mariani, and F. Marcondes, "Numerical investigation of several physical and geometric parameters in the natural convection into trapezoidal cavities," *Int. J. Heat Mass Transf.*, vol. 55, no. 23–24, pp. 6808–6818, Nov. 2012. DOI: [10.1016/j.ijheatmasstransfer.2012.06.088](https://doi.org/10.1016/j.ijheatmasstransfer.2012.06.088).
- [46] T. Basak, S. Roy, and I. Pop, "Heat flow analysis for natural convection within trapezoidal enclosures based on heatline concept," *Int. J. Heat Mass Transf.*, vol. 52, no. 11–12, pp. 2471–2483, Nov. 2009. DOI: [10.1016/j.ijheatmasstransfer.2009.01.020](https://doi.org/10.1016/j.ijheatmasstransfer.2009.01.020).
- [47] N. I. Tracy and D. W. Crunkleton, "Oscillatory natural convection in trapezoidal enclosures," *Int. J. Heat Mass Transf.*, vol. 55, no. 17–18, pp. 4498–4510, Aug. 2012. DOI: [10.1016/j.ijheatmasstransfer.2012.03.036](https://doi.org/10.1016/j.ijheatmasstransfer.2012.03.036).
- [48] S. A. M. Mehryan, M. Ghalambaz, R. K. Feeoj, A. Hajjar, and M. Izadif, "Free convection in a trapezoidal enclosure divided by a flexible partition," *Int. J. Heat Mass Transf.*, vol. 149, pp. 119186, Mar. 2020. DOI: [10.1016/j.ijheatmasstransfer.2019.119186](https://doi.org/10.1016/j.ijheatmasstransfer.2019.119186).
- [49] R. U. Haq, S. N. Kazmi, and T. Mekkaoui, "Thermal management of water based SWCNTs enclosed in a partially heated trapezoidal cavity via FEM," *Int. J. Heat Mass Transf.*, vol. 112, pp. 972–982, Mar. 2017. DOI: [10.1016/j.ijheatmasstransfer.2017.05.041](https://doi.org/10.1016/j.ijheatmasstransfer.2017.05.041).
- [50] R. U. Haq and S. Aman, "Water functionalized CuO nanoparticles filled in a partially heated trapezoidal cavity with inner heated obstacle: FEM approach," *Int. J. Heat Mass Transf.*, vol. 128, pp. 401–417, Jan. 2019. DOI: [10.1016/j.ijheatmasstransfer.2018.08.088](https://doi.org/10.1016/j.ijheatmasstransfer.2018.08.088).
- [51] H. Saleh, R. Roslan, and I. Hashim, "Natural convection heat transfer in a nanofluid-filled trapezoidal enclosure," *Int. J. Heat Mass Transf.*, vol. 54, no. 1–3, pp. 194–201, Jan. 2011. DOI: [10.1016/j.ijheatmasstransfer.2018.08.088](https://doi.org/10.1016/j.ijheatmasstransfer.2018.08.088).
- [52] M. H. Esfe, A. A. A. Arani, W. Yan, H. Ehteram, A. Aghaie, and M. Afrand, "Natural convection in a trapezoidal enclosure filled with carbon nanotube–EG–water nanofluid," *Int. J. Heat Mass Transf.*, vol. 92, no. 1–3, pp. 76–82, Jan. 2016. DOI: [10.1016/j.ijheatmasstransfer.2015.08.036](https://doi.org/10.1016/j.ijheatmasstransfer.2015.08.036).
- [53] Z. Ghoben and A. K. Hussein, "The natural convection inside a 3D triangular cross section cavity filled with nanofluid and included cylinder with different arrangements," *Diagnostyka*, vol. 23, no. 2, pp. 1–13, 2022. DOI: [10.29354/diag/149734](https://doi.org/10.29354/diag/149734).
- [54] A. K. Hussein, "Entropy generation due to the transient mixed convection in a three-dimensional right-angle triangular cavity," *Int. J. Mech. Sci.*, vol. 146–147, pp. 141–151, Oct. 2018. DOI: [10.1016/j.ijmecsci.2018.07.012](https://doi.org/10.1016/j.ijmecsci.2018.07.012).
- [55] H. Laouira, F. Oudina, A. K. Hussein, L. Kolsi, A. Merah, and O. Younis, "Heat transfer inside a horizontal channel with an open trapezoidal enclosure subjected to a heat source of different lengths," *Heat Transf. Asian Res.*, vol. 49, no. 1, pp. 406–423, Jan. 2020. DOI: [10.1002/hjt.21618](https://doi.org/10.1002/hjt.21618).
- [56] A. Kareem, H. Mohammed, A. K. Hussein, and S. Gao, "Numerical investigation of mixed convection heat transfer of nanofluids in a lid-driven trapezoidal cavity," *Int. Commun. Heat Mass Transf.*, vol. 77, pp. 195–205, Oct. 2016. DOI: [10.1016/j.icheatmasstransfer.2016.08.010](https://doi.org/10.1016/j.icheatmasstransfer.2016.08.010).
- [57] M. S. Hossain and M. A. Alim, "MHD free convection within trapezoidal cavity with non-uniformly heated bottom wall," *Int. J. Heat Mass Transf.*, vol. 69, pp. 327–336, Feb. 2014. DOI: [10.1016/j.ijheatmasstransfer.2013.10.035](https://doi.org/10.1016/j.ijheatmasstransfer.2013.10.035).
- [58] N. S. Gibanov, M. A. Sheremet, and I. Pop, "Free convection in a trapezoidal cavity filled with a micropolar fluid," *Int. J. Heat Mass Transf.*, vol. 99, pp. 831–838, Aug. 2016. DOI: [10.1016/j.ijheatmasstransfer.2016.04.056](https://doi.org/10.1016/j.ijheatmasstransfer.2016.04.056).
- [59] S. Ahmed, A. K. Hussein, M. Mansour, Z. Raizah, and X. Zhang, "MHD mixed convection in trapezoidal enclosures filled with micropolar nanofluids," *Nano Sci. Technol. Int. J.*, vol. 9, no. 4, pp. 343–372, 2018. DOI: [10.1615/NanoSciTechnolIntJ.2018026118](https://doi.org/10.1615/NanoSciTechnolIntJ.2018026118).
- [60] F. Ali, H. Hamzah, A. K. Hussein, M. Jabbar, and P. Talebizadehsardari, "MHD mixed convection due to a rotating circular cylinder in a trapezoidal enclosure filled with a nanofluid saturated with a porous media," *Int. J. Mech. Sci.*, vol. 181, pp. 105688, Sep. 2020. DOI: [10.1016/j.ijmecsci.2020.105688](https://doi.org/10.1016/j.ijmecsci.2020.105688).
- [61] A. K. Hussein, H. Hamzah, F. Ali and L. Kolsi, "Mixed convection in a trapezoidal enclosure filled with two layers of nanofluid and porous media with a rotating circular cylinder and a sinusoidal bottom wall," *J. Therm. Anal. Calorim.*, vol. 141, no. 5, pp. 2061–2079, Sep. 2020. DOI: [10.1007/s10973-019-08963-6](https://doi.org/10.1007/s10973-019-08963-6).
- [62] ANSYS, "ANSYS Fluent User's Guide 2020R2," 2020.
- [63] S. V. Patankar, *Numerical Heat Transfer and Fluid Flow*. Washington, DC: Hemisphere, 1980.
- [64] A. Bejan, *Convection Heat Transfer*. New York, NY: John Wiley Sons Inc., 1984.